International Journal for Innovative Engineering and Management Research
PEER REVIEWED OPEN ACCESS INTERNATIONAL JOURNAL
www.ijiemr.org

ENHANCED DUAL-BATTERY ELECTRIC VEHICLE OPERATION USING A RECONFIGURABLE FOPID-CONTROLLED POWER CONVERTER

Dr. K. Srinivas[1], T. Naresh[2]
[1]Professor & Vice Principal , Department of Electrical and Electronics Engineering, JNTUH University College of Engineering (Autonomous), Jagtial, Telangana,India.
[2]PG, M.Tech (Electrical Power Systems), Department of Electrical and Electronics Engineering, JNTUH University College of Engineering (Autonomous), Jagtial, Telangana, India.

Abstract: An electric vehicle (EV) reconfigurable power converter based on fractional-order proportional-integral-derivative (FOPID) theory is the intended outcome of this project's modelling and management efforts. two batteries may be charged simultaneously. Having the capacity to charge and traction with two batteries in different modes (series, parallel, independent) improves system dependability and operational flexibility. Safe functioning in parallel and suppression of circulating currents between battery units are ensured by an intrinsic voltage balancing system. One may assess the converter's dynamic behaviour using theoretical modelling that makes use of state-space averaging and small-signal analysis. Swapping out the traditional PI controller with a FOPID one may boost the system's resilience, dynamic responsiveness, and steady-state performance over a wide range of operating situations. We run simulations in MATLAB/Simulink to assess the suggested control technique. Results show that compared to the standard PI-based control strategy, the proposed method performs much better.

Key terms_ Electric traction systems, series-parallel battery architecture, energy efficiency, robust control, voltage balancing, small-signal analysis, and battery management systems (BMS) are common words used when discussing electric cars.

I. INTRODUCTION

More and more people throughout the world are looking for renewable energy sources that won't hurt people or the planet because of the rising pollution levels. In 2022, the transportation sector was accountable for over 20% of CO_2 emissions worldwide and around 29% of these emissions in the United States [1]. The immediate results of this paradigm change are a decrease in demand for traditional ICE cars and an increase in interest in electric vehicles. More than 86% of all vehicles will be electric by 2022, up from 3% in 2010 [2], making Norway one of the countries where this shift will be most apparent.

Electric vehicles have several benefits, including reduced environmental effect, increased energy efficiency, less noise pollution, lower running costs, and fewer maintenance needs. There are still a lot of questions concerning their durability, lengthier charging periods, expensive starting pricing, and range that prevent them from being widely used. To fix these problems, many people have proposed several solutions, but each of them has its own set of drawbacks.These include improved battery technology, faster charging infrastructure, and solutions for exchanging batteries. Concerning the practicality of high-capacity battery systems, the availability of necessary infrastructure, and the need for standardization, battery switching poses distinct obstacles [3].

Dual energy storage systems (DESS), particularly those that use two batteries, have attracted a lot of interest as a possible way to overcome these restrictions. A number of chemists have been investigated in the past with the hopes of developing hybrid battery ultra-capacitor and dual-battery systems that increase power density, battery life, and driving range [4]-[22]. Ultra-capacitors don't have a very high energy density, and most systems that use two batteries aren't very flexible. Despite the significance of dynamic reconfiguration, the ability to charge and traction batteries in parallel, series, or independently is Overlooked in the current research.Some examples of recent innovations in electric vehicle design include patented systems [24]-[32] and programmable dual-battery arrangements, which have found use in two-wheeler

International Journal for Innovative Engineering and Management Research
PEER REVIEWED OPEN ACCESS INTERNATIONAL JOURNAL
www.ijiemr.org

applications[23].Although these technologies provide a lot of operational flexibility, they don't always account for things like efficient charging procedures, coordinated energy transfer, and complicated control systems. Most voltage balancing systems rely on resistive dissipation, which reduces the efficiency of the system. In response to these issues, researchers have developed reconfigurable dual-battery power converter topologies [33]. As an added bonus, these topologies can handle high-voltage applications that need a series connection as well as high-current needs that are better met by a parallel connection, all while still maintaining single-battery operation. These combinations improve performance and flexibility; how successful they are, however, is heavily dependent on the control strategy used. Despite their widespread use, classic proportional-integral (PI) controllers lack the adaptability necessary to handle nonlinearities, dynamic factors, and unforeseen operational circumstances.

This paper presents a reconfigurable power converter for electric vehicle applications that use FOPID controllers. Users may choose between charging and traction modes that employ series, parallel, or freestanding batteries using the proposed technology. Preventing potentially dangerous parallel operation and circulating currents across batteries is achieved by the use of an inbuilt voltage balancing system. Our model improves upon previous efforts to represent the converter's dynamics by combining state-space averaging with small-signal analysis. Better resilience, dynamic responsiveness, and steady-state performance are achieved by the FOPID controller compared to traditional PI controllers due to the increased number of degrees of freedom achieved by the use of fractional orders. To better manage ambiguity and nonlinearity in EV power conversion systems, this technique is suggested. The suggested design is a two-stage charging architecture that consists of a DC-DC buck converter and a Totempole PFC stage. This setup allows for the simultaneous charging of two batteries, either in series or parallel. Enhanced energy management, longer battery life, and less heat stress are just a few of the many advantages of the method. The suggested control method has been validated by hardware implementation and MATLAB/Simulink simulations. Compared to traditional PI-based control, our system performs better in terms of stability, tracking precision, and transient responsiveness.

II. PROPOSED SYSTEM

The block diagram of a suggested inverter-charger system (ICS) is shown in Figure 1(a). This system integrates a rectifier for use during battery charging and an inverter for use when the vehicle is moving. Figure 1(b) shows that in order to evaluate the many aspects of the suggested topologies, the ICS is set up in a thorough circuit design. As can be seen in Figure 1, the system is clearly not isolated. One possible way to verify the hypothesis is with a standalone ICS that can use two batteries. Figure 2(a) and (b) show the two energy storage source converters' complete circuit layout. Because contactors make up the bulk of the architecture in Figure 2(a), it is called a contactor-based converter (CBC). Since most of the components in Figure 2(b) are switches that can be turned in either direction, this design is also called a bidirectional switch-based converter (BSC).

Figure 1(b) shows the three-legged ICS. Two 3PST switches AND one SPDT switch round out the circuit. There are also have two inductors and two capacitors. The semiconductor switches for the first two legs, the third and fourth legs, and the third and sixth legs are S1c, S2c, S3c, and S4c, respectively. When an electric vehicle is at rest, the integrated circuit switches into a three-phase traction inverter; however, when the vehicle is moving, it switches into a two-stage, non-isolated charger. Unlike S3c and S4, which function at line frequency, S1c, S2c, S5c, and S6 have high switching frequencies and are used as chargers. To put it more simply, while the charging mode is active, the ICS may switch between two conversion modes: one that uses the first and second legs to form a totem-pole Power Factor Correction (PFC) converter, and another that, if preferred, operates as a buck converter. In traction inverter mode, the ICS mimics the operation of a three-phase inverter by quickly cycling the switches on each of the three legs. Although the 3PST-1 switch is active when the device is charging, you could notice that the 3PST-2 switch is off. Remember that the SPDC switch's location determines whether the ICS system may be configured to charge with or without the buck converter. You may disable the buck converter by moving the SPDT switch to position I if the voltage of the batteries is higher than 1.15 times the peak voltage of the grid. To activate the buck converter, turn the SPDT switch to position H when the battery voltage falls below 1.15 times the peak AC voltage. This setup allows you to charge batteries with a broad

International Journal for Innovative Engineering and Management Research
PEER REVIEWED OPEN ACCESS INTERNATIONAL JOURNAL
www.ijiemr.org

variety of input voltages. You may already know that ICS can enable features like V2G, V2V, and V2L (vehicle-to-load) by acting as a bidirectional converter. Reactive power control and classical inverter control are also possible with a single load using unipolar sinusoidal pulse width modulation (PWM), even though ICS systems achieve active power management using Totempole switching.

One inductor (L), two capacitors (C1 and C2), two high-frequency power diodes (D1 and D2), three contactors (CT1, CT2, and CT3), and two integrated gate bipolar transistors (IGBTs) with antiparallel diodes make up the CBC topology converter, as shown in Figure 2(a). You can see all the potential uses of this converter in Figure 3. Figure 4(a) and (b) depict the possible modes of operation of the CBC when terminal AB is coupled to a single BP, such BP-1 or BP-2. As shown in Figure 3(c) or 3(d), the CBC configuration may be used with two BPs connected in series or parallel to provide a greater output voltage at terminal AB or faster charging capabilities. Figure 3(d) is used in lieu of this when a greater current is required to attain the required BP terminal voltage, as is the case when charging at double the regular pace or while accelerating. To transmit power from a high-voltage BP to a low-voltage one, the CBC design acts as a voltage-balancing buck converter, as shown in Figure 4.3(e). Switch S2 stays off the whole time, however switch S1 is rapidly switched on and off if BP-1's voltage is greater than BP-2's. If you swap out the diodes D1 and D2 in Figure 3(e) with programmable switches (MOSFET/IGBT), you may use the CBC to transfer power from a low-voltage BP to a high-voltage one. When the two batteries' charge levels (or terminal voltages) are very different, two solutions may be suggested:

1) If the electric vehicle is kept off for an extended period of time, the energy may be transferred from the fully charged battery to the partially charged battery.

2) Use the charged battery for propulsion while you're not moving by switching between the lower-state and higher-state batteries. The method necessitates a bidirectional converter, which may be achieved by substituting MOSFETs or IGBTs for D1 and D2. The electric car may now exclusively use the higher system on chip in its battery pack as a result of this modification.

The dual-battery system may be optimized for performance and lifespan by including one of these systems, which can efficiently handle huge voltage differentials and provide smooth energy transfer between the batteries.

Figure 2(b) depicts the BSC design, which includes an inductor L, two conventional switches S1 and S2, three bidirectional switches S3–S5, and two diodes D1 and D2.

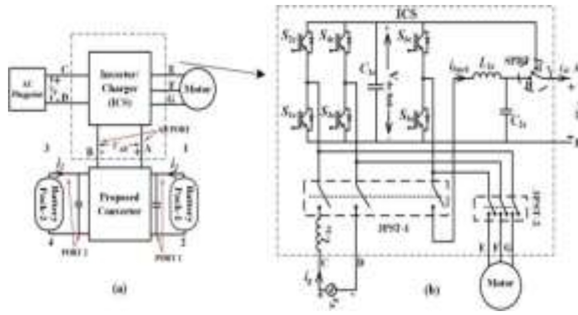

Fig1.The suggested converter is shown schematically connected to an integrated charger power source with batteries

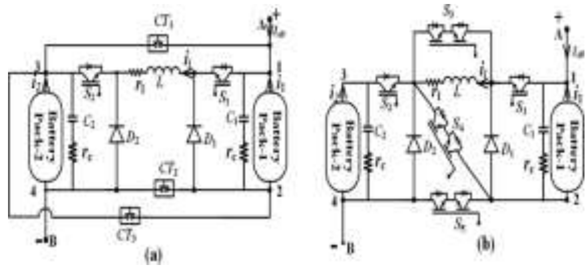

Fig. 2. Both the contactor-based converter Figure (a) and the bidirectional switch-based converter Figure (b) display their respective circuit layouts.

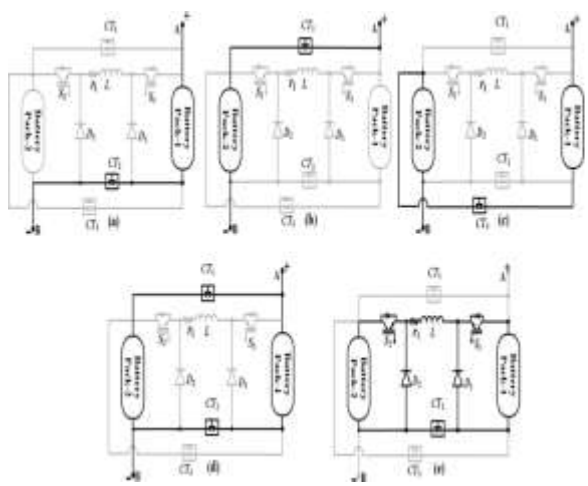

International Journal for Innovative Engineering and Management Research
PEER REVIEWED OPEN ACCESS INTERNATIONAL JOURNAL
www.ijiemr.org

Fig. 3. Different Types of CBC Operation (a) BP-1's Independent Operation, (b) BP-2's Independent Operation, (c) A voltage-balancing system; (d) Two BPs connected in series; and (e) Two BPs connected in parallel.

III.DYNAMIC MODEL AND CONTROLLER DESIGN:

Controllers and dynamic models should be included throughout the design process of electric vehicle power electronic systems to ensure their reliability and cost-effectiveness. A new reconfigurable power converter with two batteries may have its voltages, currents, and power flow analyzed using dynamic modelling to see how these variables vary over time. The stability and efficiency of electric cars depend on precise modelling of their system dynamics due to the high degree of dynamic nature of their operation, which encompasses acceleration, deceleration, regenerative braking, and charging modes. An inverter-fed traction motor, two batteries, a DC bus capacitor, and a reconfigurable bidirectional DC-DC converter are all components of the suggested dynamic model for a system including electric vehicles with twin batteries. By modelling them in a similar circuit, we can accurately depict the voltage variations of each battery with respect to their charge state and load current. This circuit has an open-circuit voltage source and an internal resistance. Different switching configurations are used to produce a set of state-space equations that describe the reconfigurable power converter. In order to analyse both transient and steady-state activity, these equations explain the relationship between inductor currents, capacitor voltages, and switching states.

It is common practice to use state-space averaging methods when trying to model the converter's dynamics in a high-frequency switching context. A continuous-time model, appropriate for control system design, is produced by averaging the switching states throughout one switching period. The averaged model captures important system dynamics while reducing computing complexity. Designers may use this method to assess the system's stability, reactivity, and sensitivity to changes in parameters. The dynamic equations produced demonstrate that variations in duty cycle obviously affect the DC bus voltage and power sharing between the two batteries.

Reliable regulation of the DC bus voltage and efficient power management between the two batteries begin with a well-designed controller. The fundamental goal of the control is to keep the DC bus voltage constant, regardless of changes in load demand or battery conditions. Determining how much current each battery may drain depending on its charge, health, and power capacity is another goal. A closed-loop control system is used to accomplish these goals by gathering feedback data from many sources, such as the DC bus voltage, inductor current, and battery current, among others. One common component of power electronic systems is the proportional-integral (PI) controller, which is well-liked for its efficacy and simplicity. In order to regulate the DC bus voltage, the suggested solution employs a PI controller. By comparing the current voltage to a reference DC bus, the controller can figure out the correct duty cycle for the reconfigurable converter. A quick transient response with little overshoot and no steady-state inaccuracy is provided by PI controller settings that have been properly calibrated. The converter and batteries may be safeguarded by configuring current control loops to restrict peak currents. The reconfiguration of the converter may be supervised using a mix of traditional control methods and controllers based on logic and rules. The controller takes into account variables including vehicle speed, load demand, and battery charge level while deciding which converter mode to use. Buck, boost, and bidirectional operation are variables that fall within this category. The controller prevents the batteries from becoming overcharged while regenerative braking is on. With this smart mode selection, the system's resilience and adaptability are enhanced. We verify the controller design and dynamic model with MATLAB/Simulink simulations. Even when the demand fluctuates quickly, the results show that the DC bus voltage stays the same and that the two batteries can exchange power effectively. The controller ensures that the system may transition between modes of operation without causing instability or overworking its components. Based on dynamic modelling and controller design, the suggested reconfigurable power converter system ensures efficient, stable, and dependable performance in electric vehicle applications. The ICS converter, which is used as an onboard charger for electric cars, consists of a Totempole PFC converter and, if desired, a Buck converter. In their suggested forms, CBC and BSC converters are functionally similar.

International Journal for Innovative Engineering and Management Research
PEER REVIEWED OPEN ACCESS INTERNATIONAL JOURNAL
www.ijiemr.org

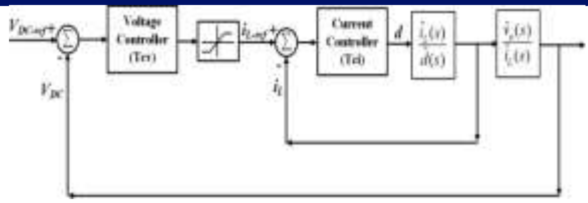

Fig. 4.The power converter's dual loop control is shown in the block diagram.

TABLE I

Relay-Charger System Parameters (ICS)

S. No	Parameter	Specification
1	Switching Frequency	20 kHz
2	Input Voltage/ Grid Voltage (V_g)	60-70V(rms)
3	L_{1c}, L_{2c}	1 mH, 0.25mH
4	C_{1c}, C_{2c}	2000 uF, 20 uF
5	S_{1c}, S_{2c}, S_{3c}, S_{4c}, S_{5c} and S_{6c}	600V, 75A
6	$V_{dc\ link}$	130V
7	V_{AB}	36V
8	Power rating of converter	500W

Buck converters in voltage-balancing mode. Figure 4 shows how the front-end converter (totempole converter) controls the inner loop current and the outer loop voltage using a dual-loop control mechanism. Depending on the grid voltage, one component of the ICS, the totem-pole boost PFC, has a varied switch topology and a variable duty ratio similar to a traditional boost converter. The architecture of the boost converter is therefore used in dynamic modelling and parameter design.

$$\frac{\widehat{i_g}(s)}{\widehat{d}(s)} = \frac{1.3013 \times 10^5(s + 29.57)}{s^2 + 77.1s + 1.903 \times 10^5} \quad (1)$$

The Bode plot generated for (1) is shown in Figure 4.5. The frequency that clearly indicates a crossover is 1.3×10^1 rad/s.

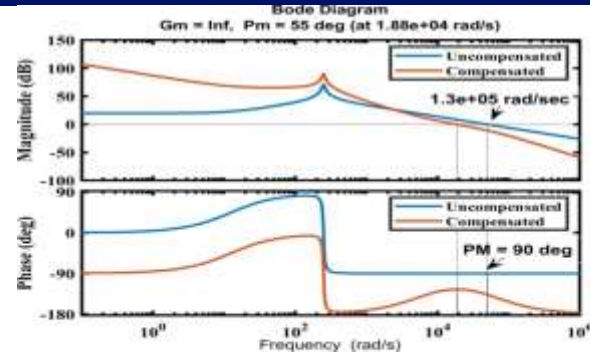

Fig. 5. Uncompensated versus compensated systems' Bode plots

when the frequency goes over the switching threshold of 1.25×10^1 rad/s, it disrupts the system. Consequently, the K-factor approach is used while building a type-2 compensator. To enhance stability and avoid overshoot, the compensator was designed with a phase buffer of 55 degrees. To achieve both quick reaction and greater stability, a crossover frequency of 3000 Hz (1.88×10^1 rad/s) was chosen. In this design of compensator and controller, the function that transfers control is:

$$T_{ci\_tpc} = \frac{8617.5(s + 5969)}{s(s + 5.952 \times 10^4)} \quad (2)$$

Analyse Figure 5 shows bode plot. The desired compensator has successfully attained the requisite phase margin at the specified crossover frequency. The DC link voltage Vdc˙link may be controlled via a two-loop system, with the inner loop specifically designed to regulate current. Table II's parameters and small-signal modelling were used to produce the following voltage control plant transfer function:

$$\frac{\widehat{v_{C1c}}(s)}{\widehat{i_g}(s)} = \frac{-1077.2(s + 2.501 \times 10^4)}{(s + 29.52)(s + 1.26 \times 10^4)} \times \frac{(s - 1.275 \times 10^4)(s + 5969)}{(s + 1.9 \times 10^4)(s + 2.78 \times 10^4)} \quad (3)$$

The objective phase margin should be 55 degrees and the open-loop transfer function should have a crossover frequency of 15 Hz; a type-2 compensator built using the K-factor approach can accomplish these goals [35]. For the purpose of controlling the

International Journal for Innovative Engineering and Management Research
PEER REVIEWED OPEN ACCESS INTERNATIONAL JOURNAL
www.ijiemr.org

voltage in the outer loop, the following is the formula for the compensator:

$$T_{cv\_tpc} = \frac{62.136(s+46.15)}{s(s+192.5)} \quad (4)$$

Equations (4.1) and (4.3) provide the plant transfer functions for the Totempole PFC component of the ICS. To continue in a similar line, the buck converter's ICS plant transfer duties are:

$$\frac{\widehat{i_{buck}}(s)}{\widehat{d}(s)} = \frac{5.2\times10^5(s+1.929\times10^4)}{s^2+1.929\times10^4 s+2\times10^8} \quad (5)$$

$$\frac{\widehat{v_{C2c}}(s)}{\widehat{i_{buck}}(s)} = \frac{8.3021\times10^{12}(s+1.016\times10^4)}{(s+1.7\times10^4)(s+6856)} \times \frac{1}{(s^2+1.1\times10^4 s+2.9\times10^8)} \quad (6)$$

As seen in Figure 4, the current controller for the buck converter is determined by taking into account the required crossover frequency of 3768 rd/sec (600 Hz) and the planned phase margin of 55 degrees. The type-2 designed current controller's transfer function is as follows:

$$T_{ci\_buck} = \frac{319.31(s+1.016\times10^4)}{s(s+1.554\times10^4)} \quad (7)$$

Using equation (4.6), a buck converter's type-2 outer loop voltage controller may be achieved with a 65-degree phase margin and a 94.2 rd/sec (15 Hz) crossover frequency. The controller's derived transfer function is shown below:

$$T_{cv\_buck} = \frac{23.522(s+145.7)}{s(s+60.97)} \quad (8)$$

To maintain the totempole PFC section of the ICS constant current (CC) charging mechanism for BPs, the system solely uses the inner current loop while the SPDT switch is in position I. When the Totempole PFC is not actively charging BP using a constant voltage (CV) technique, its outside voltage loop is inactive. The buck converter part of the ICS is currently unmanaged.

On the other hand, the Totempole PFC ICS component actively regulates the DC link voltage via the external voltage loop while the SPDT switch is in position H. To manage CC and CV charging of the BPs, respectively, you may switch the ICS's buck converter here between the inner and outer voltage loops.

According to Figure 3(e), the voltage balancing is accomplished by the suggested CBC and BSC converters in the same way as traditional buck converters. Ensuring a perfect voltage balance is the primary goal of the control in this case by regulating the inductor current. The final form of our transfer function is as follows:

$$\frac{\widehat{i_l}(s)}{\widehat{d}(s)} = \frac{1.2727\times10^5(s+3.704\times10^4))}{(s^2+3.704\times10^4 s+5.051\times10^8)} \quad (9)$$

An ideal type-2 current controller with a 55-degree phase margin and a crossover frequency of 12566 rd/sec (2000 Hz) is optimally constructed using the K-factor method in reference (9). The current controller that has been suggested looks like this:

$$T_{ci} = \frac{1454.1(s+1.267\times10^4))}{s(s+1.247\times10^4)} \quad (10)$$

TABLE II

Parameters of Proposed Converters

S. No	Parameter	Specification
1	Switching Frequency	20 kHz
2	L, r_l	0.33mH, 70 mΩ
3	C_1, C_2, r_c	5.4uF, 5.4uF,20 mΩ
4	BP-1, BP-2	36V,60 Ah
5	S_1, S_2 (MOSFET, IGBT)	60V,120A
6	CT_1 ,CT_2 and CT_3	200V, 120A
7	S_3, S_4, S_5 (Bidirectional Switch)	60V, 120A
8	D_1, D_2	60V, 15A
9	Power rating of converter	200W

IV. PROPOSED FOPID CONTROLLER

Due to their simplicity, ease of implementation, and effectiveness in decreasing steady-state errors, conventional proportional-integral (PI) controllers are widely used in the basic converter control architecture. However, multiport power converters—which often deal with bidirectional energy transfer and mode switches are not a good fit for PI controllers due to their limited working range, lack of linearity, and significant demand for dynamic responsiveness.

This study suggests a Fractional Order PID (FOPID) controller to replace the traditional PI controller in the converter system's control loops in order to address these issues.

A standard FOPID controller's transfer function is written as:

$$C(s) = K_p + \frac{K_i}{s^{\lambda}} + K_d s^{\mu} \qquad (11)$$

Where:

Proportional gain (Kp)
• Ki: Incremental profit
Derivative gain (Kd)
• Integral order λ (where 0 < λ ≤ 1) the order of the derivative, where 0 < μ ≤ 1.

By adjusting the gain and phase margins using the extra tuning knobs λ and μ, the system's stability and bandwidth may be improved. The FOPID controller's block diagram is seen in Figure 4.5. This controller improves upon the traditional PID design by use fractional orders for integral and derivative calculations instead of integers.

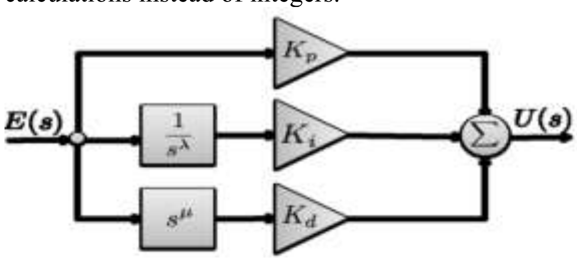

Fig.6 system for closed-loop process control based on FOPID controllers.

The use of a FOPID controller considerably enhances the stability, flexibility, and power quality of the three modes of operation for the multiport EV charger. Adding a controller transforms this system from a simple power conversion unit into an intelligent, versatile, and grid-compliant energy distribution solution that works in both urban and rural areas. This makes it perfect for situations where dependability and efficiency are of the utmost importance.

V. SIMULATION RESULTS

Additional simulation studies use a range of operating scenarios reflective of real-world electric vehicle circumstances to further assess the effectiveness of the supplied reconfigurable power converters. By integrating the suggested converter with the ICS, system-level simulations are produced in MATLAB/Simulink. The grid interface, power factor adjustment stage, DC link, reconfigurable DC-DC converter, and battery packs may all be accurately modelled using the provided framework. Using this all-encompassing modelling method, we can examine how different charging arrangements affect power flow, voltage control, and current sharing.

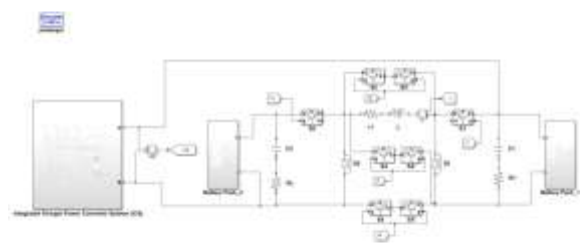

Fig 7. system's circuit in MATLAB/SIMULINK

A) EXISTING SIMULATION RESULTS (WITH PI CONTROLLER)

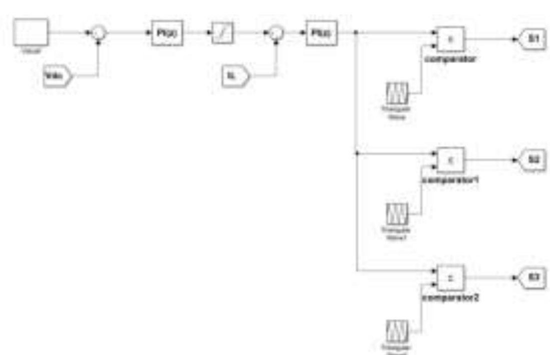

Fig.8 control circuit with a PI controller

The suggested converters were tested in a grid-to-vehicle (G2V) setup with the help of MATLAB/Simulink simulations. Keeping the DC-link voltage at 130 V and the battery current at 10 A standard allowed for charging a single battery pack (BP) utilising a 70 V (RMS) grid supply. There is little steady-state error in the DC-link voltage and battery current, as seen in Figure 9(a) and Figure 9(b), respectively.

Two BPs charged in series at 72 V are shown in Figure 9(c), while two BPs charged in parallel at 36 V are shown in Figure 9(d). The battery consumption remained constant at 20 A regardless of the mode of operation (series or parallel). These findings demonstrate that the suggested converters fully support series and parallel connections with the BPs. Changing the reference voltage at the battery terminals from 36 V to 42 V allowed us to evaluate the dynamic performance of the outer voltage controller in constant-voltage (CV) mode. Figure 9(e) shows that the same response has enough overshoot and settles quickly. In addition, as can be shown in Figure 9(f), the current controller's performance in constant-current (CC) mode, accuracy in tracking, and smooth transient behavior are all confirmed when the battery current reference is raised from 10 A to 13 A.

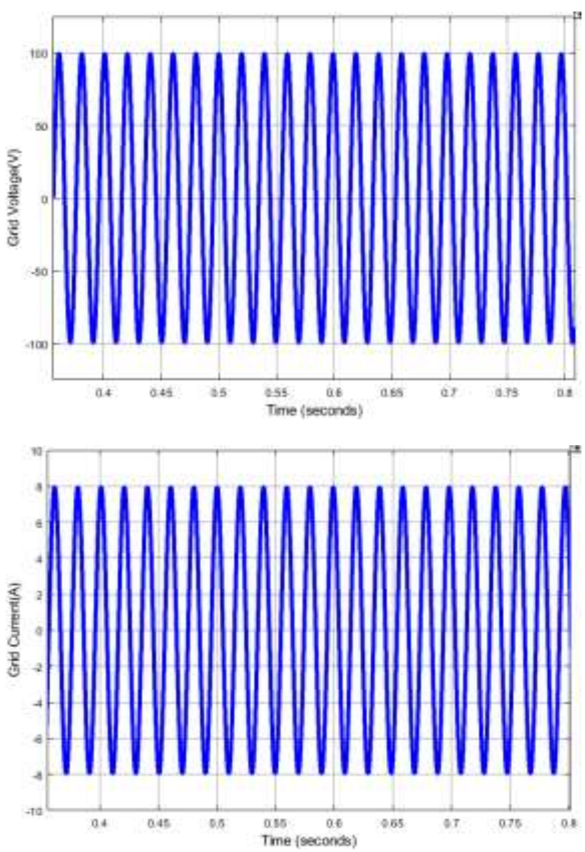

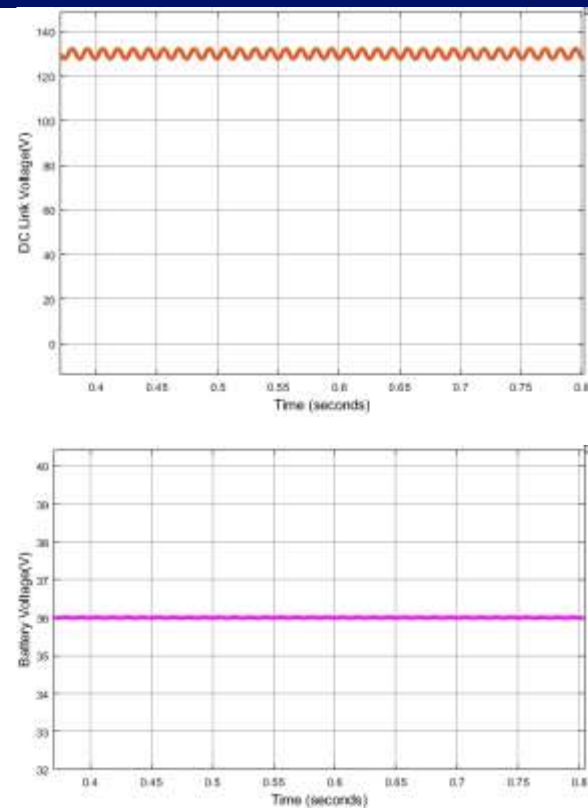

(a)

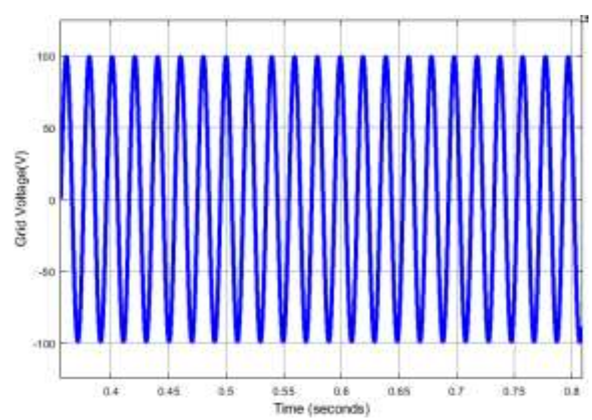

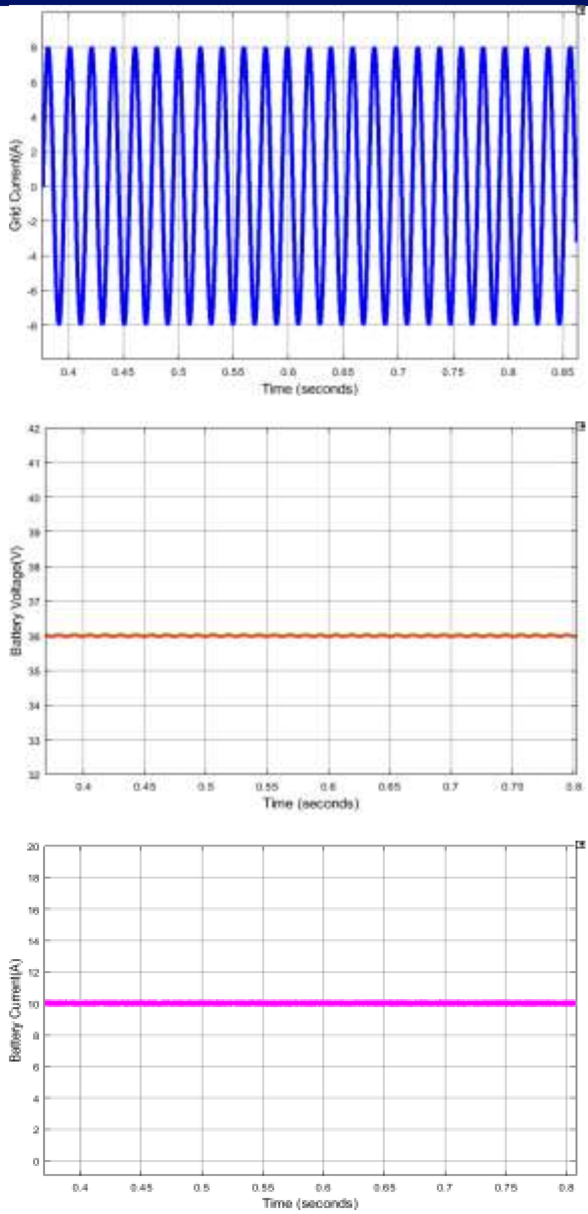
Grid Current(A)
Time (seconds)
Battery Voltage(V)
Time (seconds)
Battery Current(A)
Time (seconds)

(b)

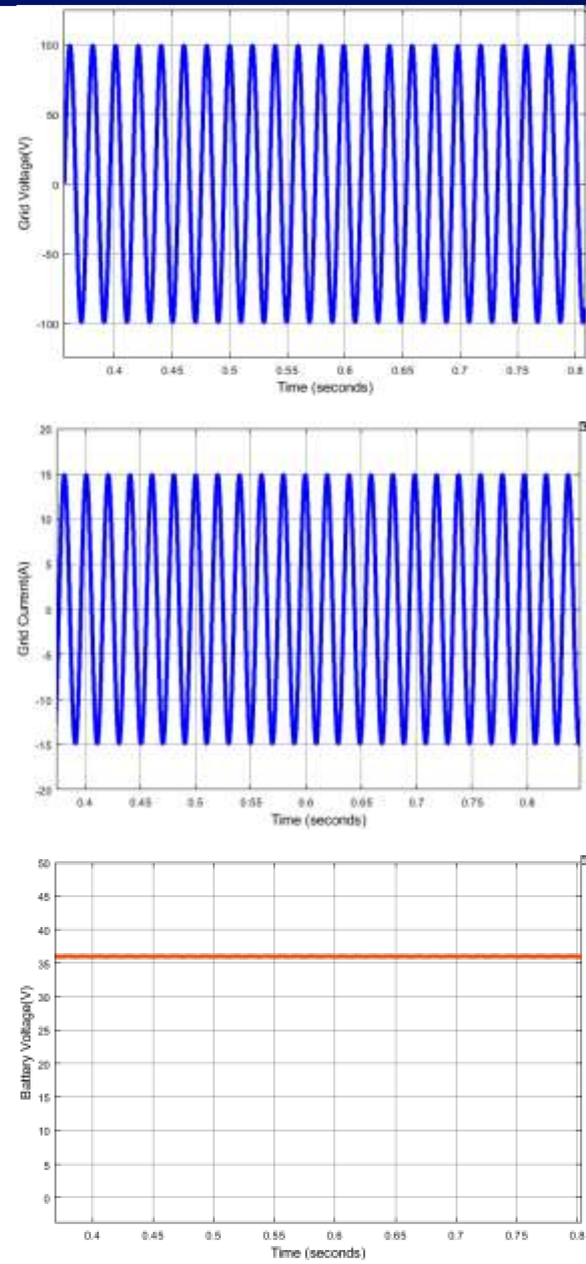
Grid Voltage(V)
Time (seconds)
Grid Current(A)
Time (seconds)
Battery Voltage(V)
Time (seconds)

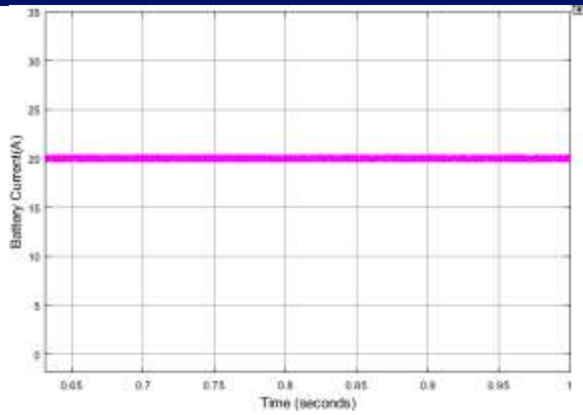
Battery Current(A)
Time (seconds)

(c)

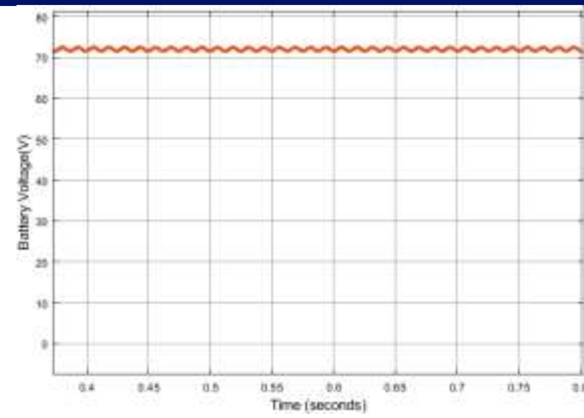
Battery Voltage(V)
Time (seconds)

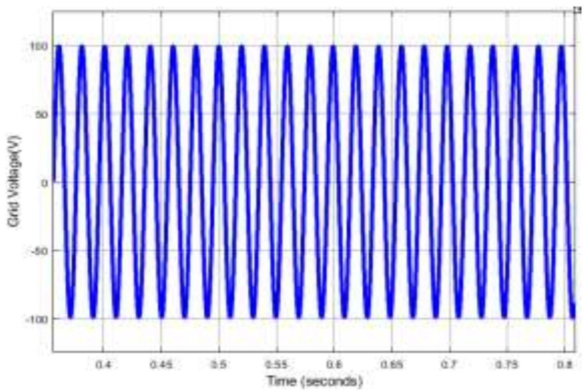
Grid Voltage(V)
Time (seconds)

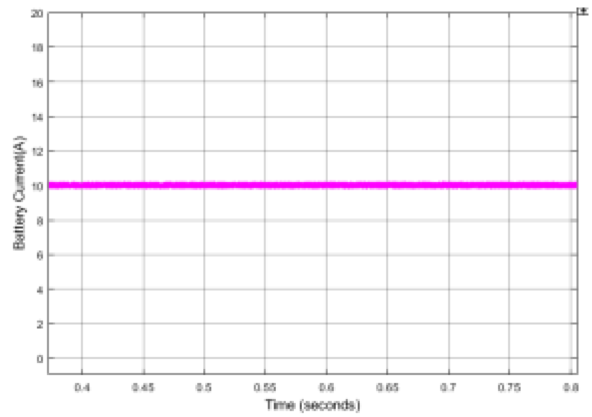
Battery Current(A)
Time (seconds)

(d)

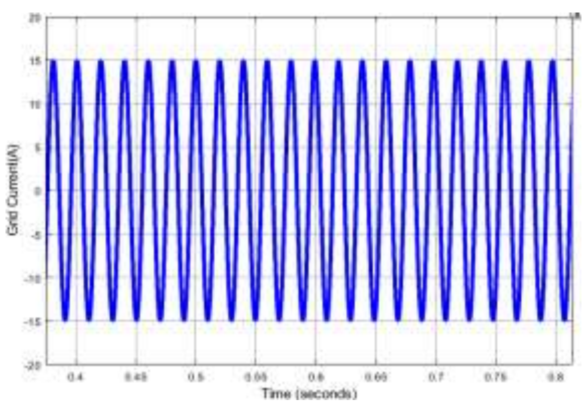
Grid Current(A)
Time (seconds)

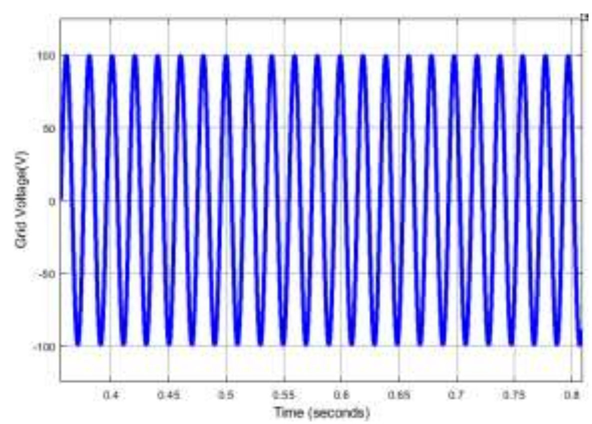
Grid Voltage(V)
Time (seconds)

International Journal for Innovative Engineering and Management Research
PEER REVIEWED OPEN ACCESS INTERNATIONAL JOURNAL
www.ijiemr.org

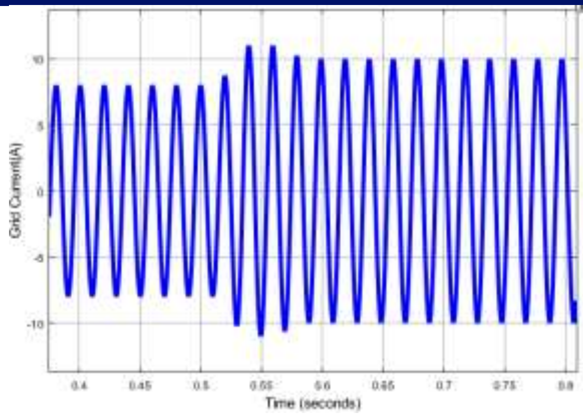

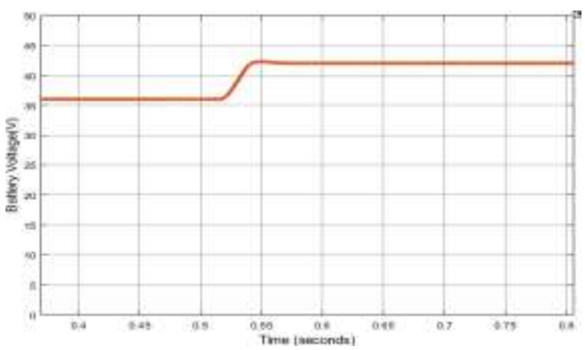

(e)

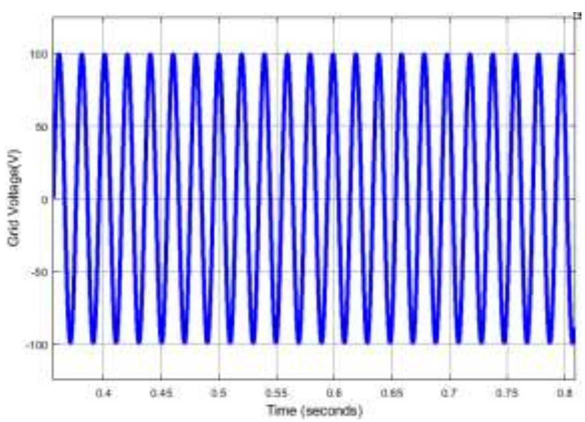

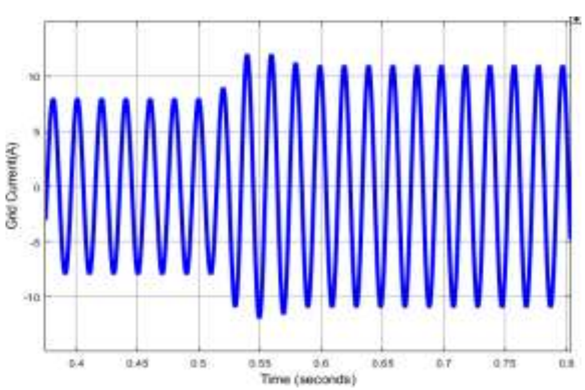

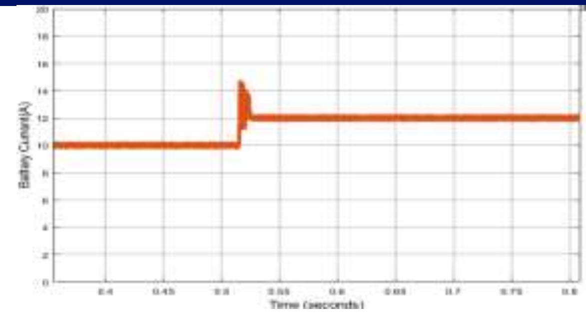

(f)

Fig.9 (a)Showing the voltages at the three terminals of the battery, dc link, and network (b)Charging just one battery at a time, (c) Powering up two batteries at once, (d) Charging two batteries in parallel, (e) Tailoring the controller's reference voltage and (f) controlling its reference current.

According to the data in Table IV, we ran simulations with BP-1's state of charge (SoC) set to 90% (terminal voltage: 41 V) and BP-2's SoC set to 30% (terminal voltage: 38 V) to guarantee that the converters we suggested could accomplish voltage balancing. We considered a 2 C charging rate and decreased the battery capacity to 3 Ah to achieve quicker voltage-balancing dynamics in a short period of time. The suggested converter used buck mode to transfer energy from BP-1 to BP-2 since their terminal voltages were greater than each other ($V_1 > V_2$). While switch S1 was toggled on and off in response to the switching frequency, switch S2 stayed in its off position under these conditions (Figure 9(e)). You can see the outcomes of the simulation in Figure 10. They prove that the battery packs' voltages are balanced since the BP-2 charging current is precisely regulated at 6 A.

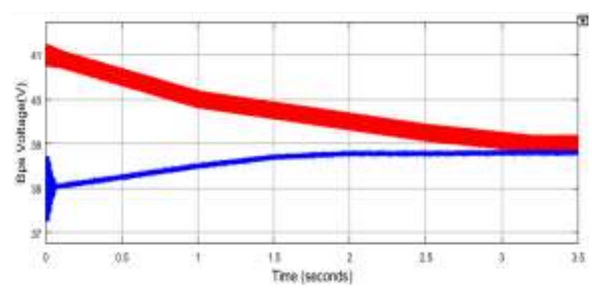

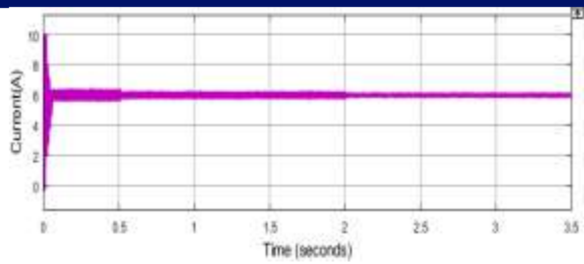

Fig.10 Simulation Result for Voltage Balancing Facility with BP's of different SoC.

B) EXTENSION SIMULATION RESULTS (WITH FOPOID CONTROLLER)

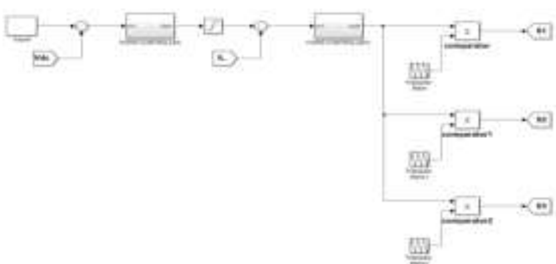

Fig.11 Using a FOPID controller for control

The suggested converters were tested in a grid-to-vehicle (G2V) setup with the help of MATLAB/Simulink simulations. Keeping the DC-link voltage at 130 V and the battery current at 10 A standard allowed for charging a single battery pack (BP) utilizing a 70 V (RMS) grid supply. See Figures 12(a) and (b) for examples of DC-link voltage and battery current that exhibit little steady-state inaccuracy. The FOPID controller is used to improve the regulation. It beats the old standard of traditional PI control in terms of both stability and dynamic responsiveness.
Charging of two BPs connected in series (72 V) and in parallel (36 V) are shown in Figure 12(d) and Figure 12(c), respectively. The battery consumption remained constant at 20 A regardless of the mode of operation (series or parallel). The FOPID controller makes sure the suggested converter can move between battery packs' series and parallel connections with ease, minimizing current ripple and increasing lifetime, when it transitions between operating modes.

Changing the reference voltage at the battery terminals from 36 V to 42 V allowed us to evaluate the dynamic performance of the outer voltage controller in constant-voltage (CV) mode. As seen in the corresponding response in Figure 12(e), the FOPID controller's increased tuning flexibility enables rapid settling with less overshoot. Results of testing the current controller in constant-current (CC) mode are shown in Figure 6.6(f) after adjusting the battery current reference from 10 A to 13 A. Providing steady transient behaviour with minimum oscillations and precise tracking, the results demonstrate that the FOPID-based control strategy is successful under dynamic operating settings.

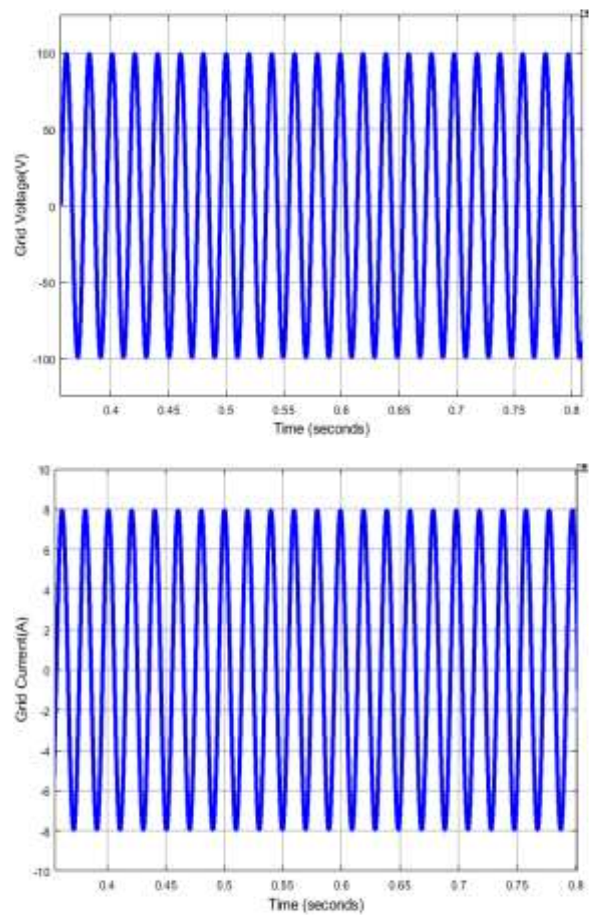

(a)

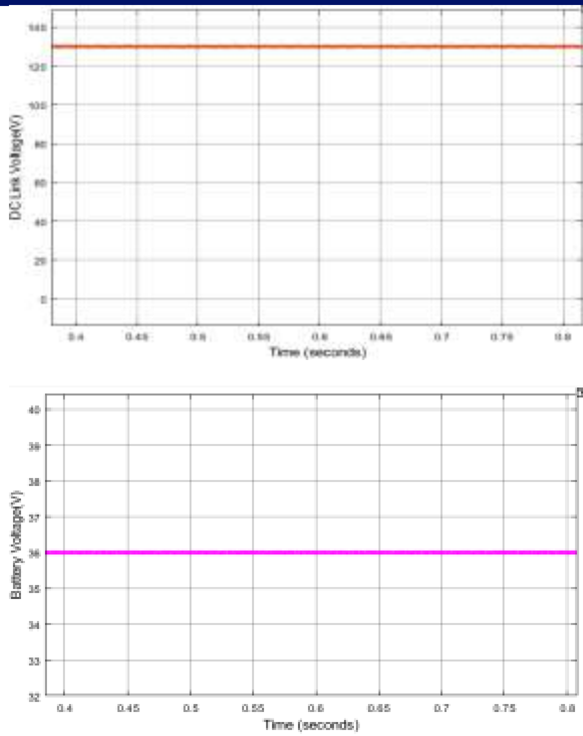
DC Link Voltage(V)
Time (seconds)
Battery Voltage(V)
Time (seconds)

(a)

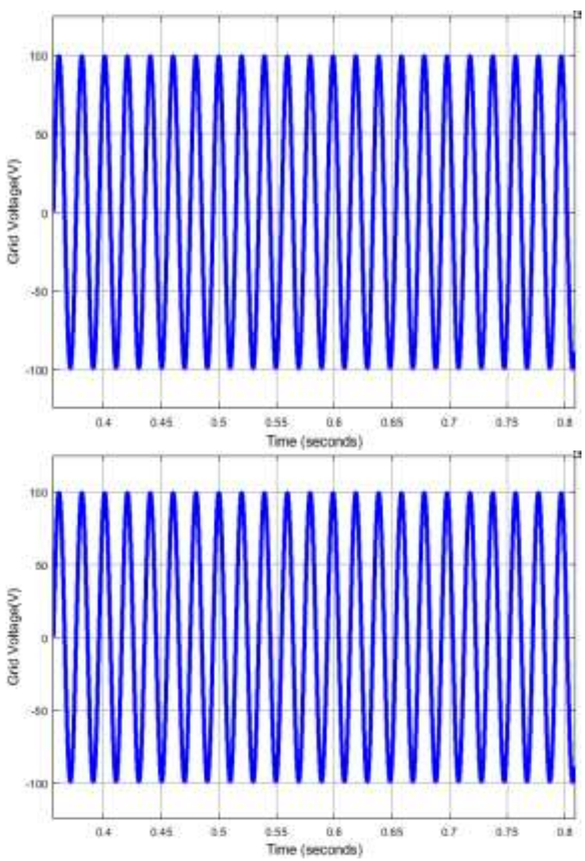
Grid Voltage(V)
Time (seconds)
Grid Voltage(V)
Time (seconds)

(b)

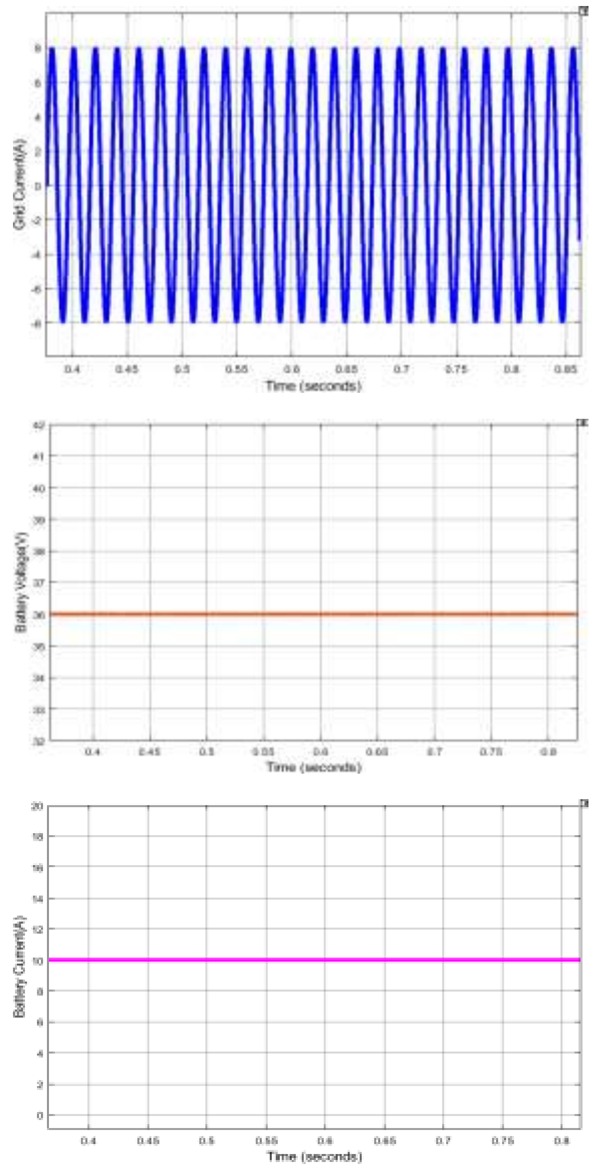
Grid Current(A)
Time (seconds)
Battery Voltage(V)
Time (seconds)
Battery Current(A)
Time (seconds)

(b)

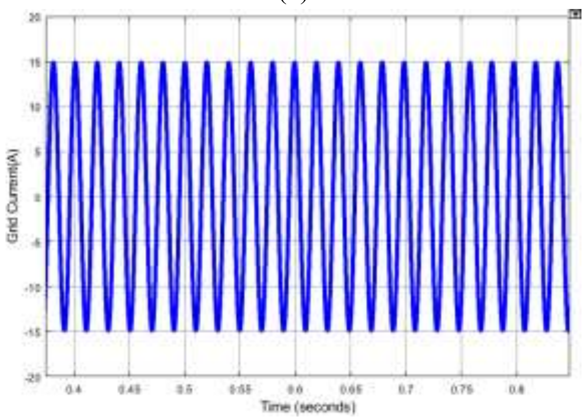
Grid Current(A)
Time (seconds)

(c)

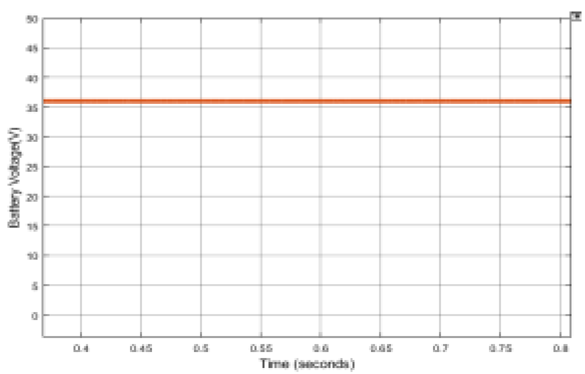
Battery Voltage(V)
Time (seconds)

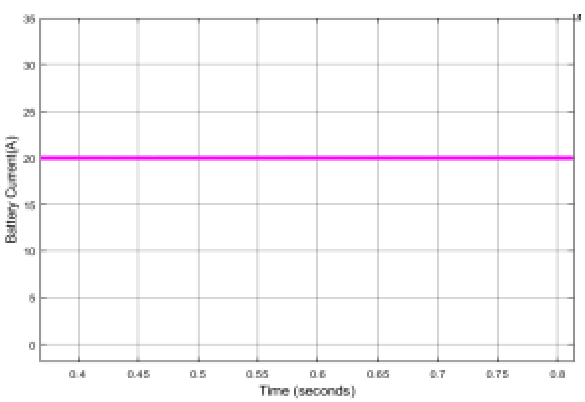
Battery Current(A)
Time (seconds)

(c)

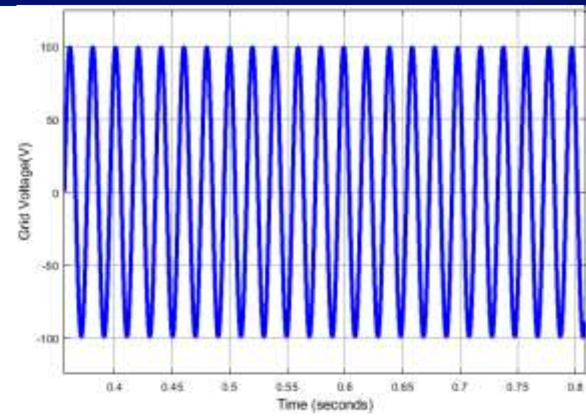
Grid Voltage(V)
Time (seconds)

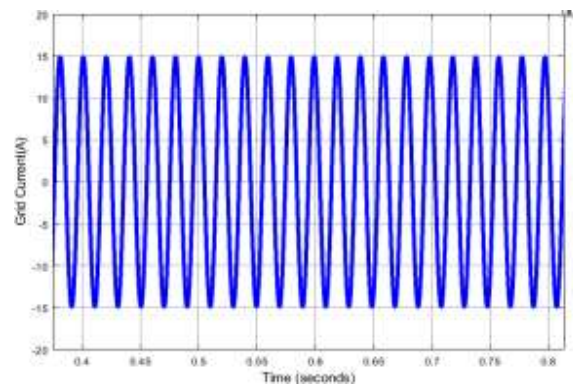
Grid Current(A)
Time (seconds)

(d)

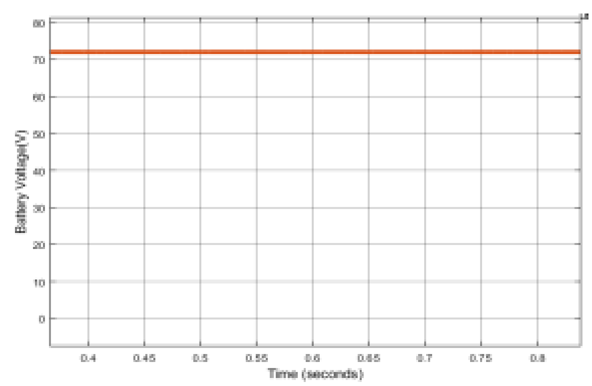
Battery Voltage(V)
Time (seconds)

International Journal for Innovative Engineering and Management Research
PEER REVIEWED OPEN ACCESS INTERNATIONAL JOURNAL
www.ijiemr.org

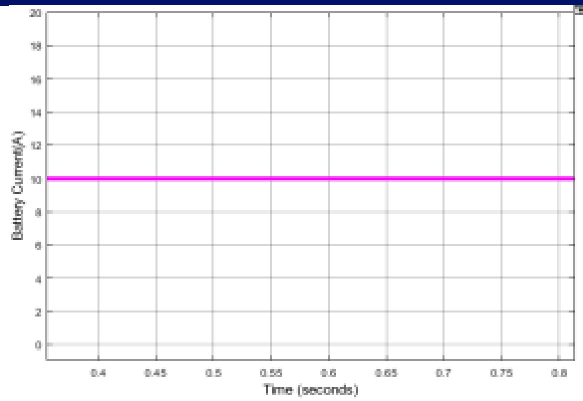

(d)

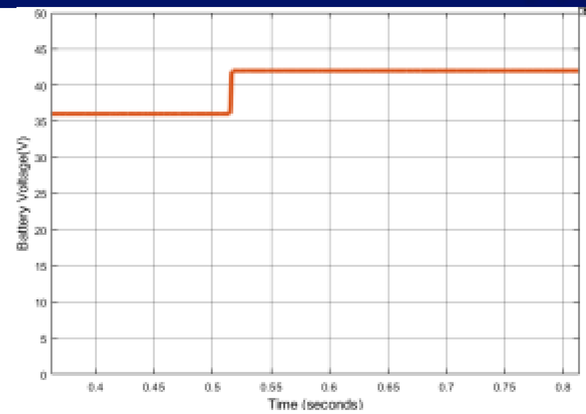

(e)

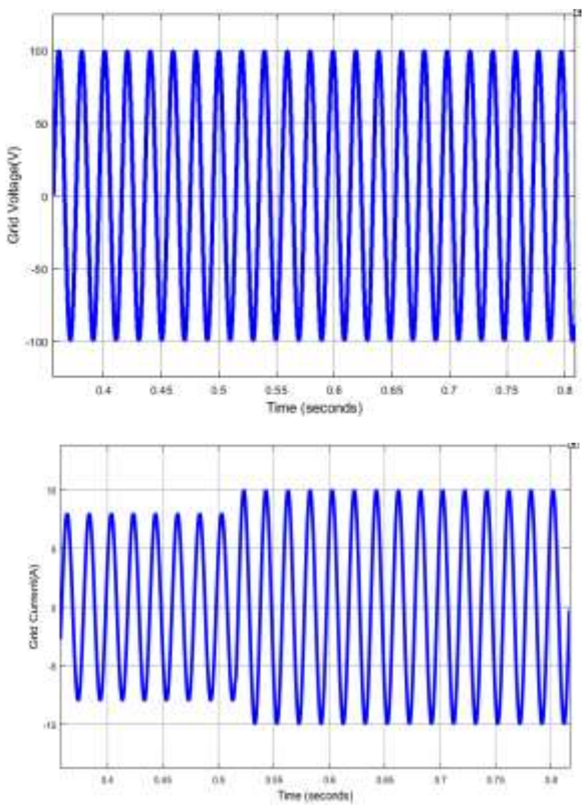

(e)

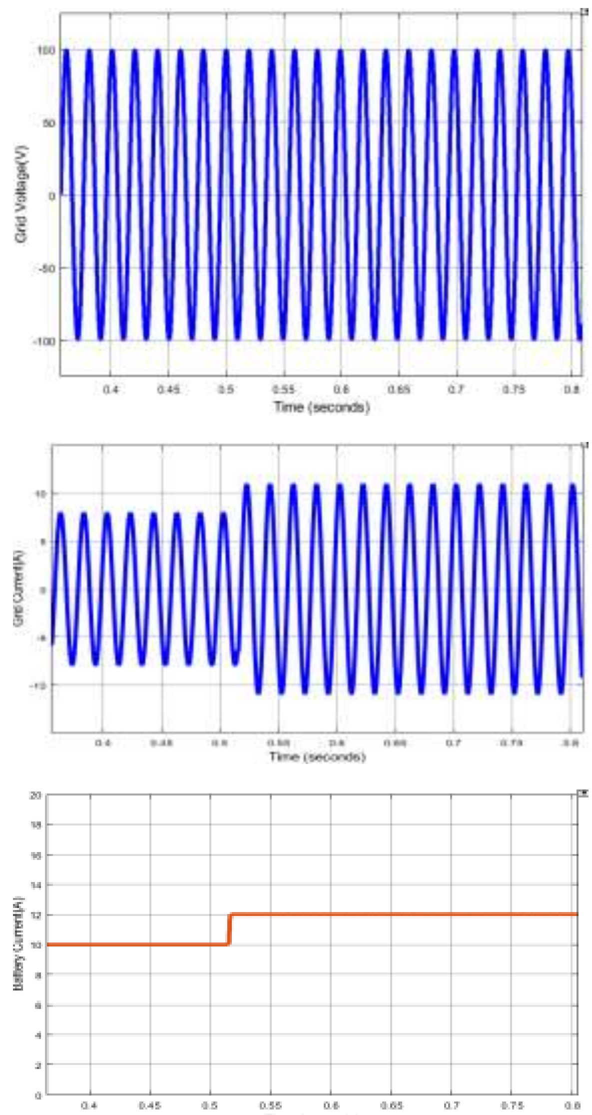

(f)

International Journal for Innovative Engineering and Management Research
PEER REVIEWED OPEN ACCESS INTERNATIONAL JOURNAL
www.ijiemr.org

Figure 12: Results of the simulation showing (a) the voltage and current on the grid, the voltage at the dc terminal, and the voltage at the battery terminals (b) Charge two batteries in series, charge two batteries in parallel, charge one battery alone, alter the voltage controller's reference voltage, and alter the current controller's reference current.

Using the characteristics mentioned in Table IV, simulations were run to evaluate the proposed converter's capability to balance voltages. Both BP-1 and BP-2 had their terminal voltages adjusted to 90% (state of charge), with BP-2 at 38 V. Reduced battery capacity to 3 Ah and 2 C charging rate allowed for faster voltage-balancing dynamics in a reduced simulation duration. The converter worked in buck mode to allow energy transfer from BP-1 to BP-2 since the terminal voltage of BP-1 was greater than that of BP-2 ($V_1 > V_2$). Using the switching frequency to control switch S1, switch S2 stayed in its OFF state, as shown in Figure 6.7(e).By replacing the traditional PI controller with a fractional order proportional-integral-derivative (FOPID) controller, the voltage-balancing mechanism became more robust and dynamic. By modulating the BP-2 charging current with extra fractional tuning choices, the FOPID controller improved tracking accuracy and transient response speed.

Figure 13 displays the simulation results, which prove that the suggested control mechanism accomplishes the target, which is a uniform voltage distribution throughout the battery packs. The FOPID-based control method shows excellent performance with reduced overshoot and improved settling time when the charging current of BP-2 is properly controlled at 6 A.

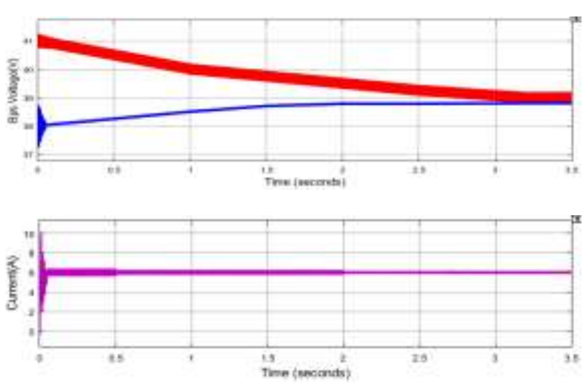

Fig. 13. Result of the Voltage Balancing Facility Simulation using BPs from various SoCs.

COMPARSION TABLE

Parameter	Existing System (PI Controller)	Extension System (FOPID Controller)
Voltage Regulation (Ripple %)	6 %	2 %
DC-Link Settling Time (Ts)	0.40 sec	0.15 sec
Overshoot (%)	18 %	8%
Rise Time (Tr)	0.20 sec	0.10 sec
Steady-State Error	2 %	0.5 %
Reference Tracking Delay	120 ms	20 – 40 ms
Voltage Balancing Time	0.8 sec	0.30 sec
SoC Mismatch Compensation Error	12 %	4 %
Transient Stability (Damping Ratio ζ)	0.6	0.9
Efficiency (%)	92 %	97 %
Dynamic Response Speed	Moderate	Fast
Controller Complexity	Low	Medium–High
Overall Performance Index (ITAE/ISE)	High (worse)	Low (better)

CONCLUSION

Two new reconfigurable power converter topologies, CBC and BSC, were introduced in this research for use in electric vehicles that utilise two batteries. The charging performance was evaluated under different operating situations using a non-isolated integrated charging system. The converters we are proposing allow for flexible reconfiguration of battery packs in series, parallel, and standalone modes, as confirmed by MATLAB/Simulink simulations. The system's efficiency was enhanced by switching from the standard PI control to a fractional-order proportional-integral-derivative (FOPID) controller. Dynamic responsiveness, tracking precision, and robustness were all enhanced in various operational scenarios by the FOPID-based control technique. In order to prevent circulating currents and prolong the life of the batteries, the built-in voltage-balancing system makes sure that the voltages of the battery packs are equal before running them in parallel. Selective connection of separate battery packs enhances system robustness, adaptability, and fault tolerance. Features such as decreased current stress, higher overall efficiency, and smooth mode switches are promising aspects of the suggested design. Although the number of components in the system has increased somewhat, the advantages in operating flexibility, dependability, and long-term cost-effectiveness outweigh this. The proposed FOPID-controlled reconfigurable converter offers a long-term, scalable, and cost-effective solution for next-generation dual-battery electric vehicle systems. It is expected to enhance energy management and lead to future smart mobility.

REFERENCES

[1] T. Esram and P. L. Chapman, "Comparison of photovoltaic array maximum power point tracking techniques," IEEE Trans. Energy Convers., vol. 22, no. 2, pp. 439–449, Jun. 2007.

[2] M. A. G. de Brito, L. P. Sampaio, G. A. Melo, and C. A. Canesin, "Evaluation of the main MPPT techniques for photovoltaic applications," IEEE Trans. Ind. Electron., vol. 60, no. 3, pp. 1156–1167, Mar. 2013.

[3] Y. Chen, X. Liu, and J. Wang, "Review of battery swapping technology for electric vehicles," IEEE Access, vol. 8, pp. 213411–213425, 2020.

[4] A. Khaligh and Z. Li, "Battery, ultracapacitor, fuel cell, and hybrid energy storage systems for electric, hybrid electric, fuel cell, and plug-in hybrid electric vehicles: State of the art," IEEE Trans. Veh. Technol., vol. 59, no. 6, pp. 2806–2814, Jul. 2010.

[5] J. Cao and A. Emadi, "A new battery/ultracapacitor hybrid energy storage system for electric, hybrid, and plug-in hybrid electric vehicles," IEEE Trans. Power Electron., vol. 27, no. 1, pp. 122–132, Jan. 2012.

[6] H. Tao, A. Kotsopoulos, J. L. Duarte, and M. A. M. Hendrix, "Transformerless high-power bidirectional DC–DC converter for fuel cell systems," IEEE Trans. Power Electron., vol. 23, no. 3, pp. 1310–1318, May 2008.

[7] F. Krismer and J. W. Kolar, "Efficiency-optimized high-current dual active bridge converter for automotive applications," IEEE Trans. Ind. Electron., vol. 59, no. 7, pp. 2745–2760, Jul. 2012.

[8] D. Aggeler, F. Canales, H. Zelaya, and O. Apeldoorn, "Ultra-fast DC-charge infrastructures for EV mobility and future smart grids," IEEE PES Innov. Smart Grid Technol., pp. 1–8, 2010.

[9] S. Dusmez and A. Khaligh, "A compact and integrated multifunctional power electronic interface for plug-in electric vehicles," IEEE Trans. Power Electron., vol. 28, no. 12, pp. 5690–5701, Dec. 2013.

[10] M. Yilmaz and P. T. Krein, "Review of battery charger topologies, charging power levels, and infrastructure for plug-in electric and hybrid vehicles," IEEE Trans. Power Electron., vol. 28, no. 5, pp. 2151–2169, May 2013.

[11] R. Teodorescu, M. Liserre, and P. Rodriguez, Grid Converters for Photovoltaic and Wind Power Systems. Hoboken, NJ, USA: Wiley, 2011.

[12] J. M. Guerrero, J. C. Vasquez, J. Matas, L. G. de Vicuna, and M. Castilla, "Hierarchical control of droop-controlled AC and DC microgrids—A general approach," IEEE Trans. Ind. Electron., vol. 58, no. 1, pp. 158–172, Jan. 2011.

[13] S. Kouro, M. Malinowski, K. Gopakumar, et al., "Recent advances and industrial applications of multilevel converters," IEEE Trans. Ind. Electron., vol. 57, no. 8, pp. 2553–2580, Aug. 2010.

[14] J. R. Vazquez, J. I. Leon, L. G. Franquelo, et al., "Model predictive control: A review of its applications in power electronics," IEEE Ind. Electron. Mag., vol. 8, no. 1, pp. 16–31, Mar. 2014.

[15] I. Podlubny, "Fractional-order systems and PIλDμ controllers," IEEE Trans. Autom. Control, vol. 44, no. 1, pp. 208–214, Jan. 1999.

[16] Y. Luo and Y. Chen, Fractional Order Motion Controls. Hoboken, NJ, USA: Wiley, 2012.

[17] C. A. Monje, Y. Chen, B. M. Vinagre, et al., Fractional-Order Systems and Controls: Fundamentals and Applications. London, U.K.: Springer, 2010.

[18] S. Das, Functional Fractional Calculus for System Identification and Controls. Berlin, Germany: Springer, 2008.

[19] R. Xiong, H. He, F. Sun, and K. Zhao, "Evaluation on state of charge estimation of batteries with adaptive extended Kalman filter," IEEE Trans. Veh. Technol., vol. 62, no. 3, pp. 1080–1088, Mar. 2013.

[20] M. Ehsani, Y. Gao, and A. Emadi, Modern Electric, Hybrid Electric, and Fuel Cell Vehicles. Boca Raton, FL, USA: CRC Press, 2010.

[21] B. Singh, S. Singh, A. Chandra, and K. Al-Haddad, "Comprehensive study of power quality problems and mitigation techniques," IEEE Trans. Ind. Electron., vol. 54, no. 5, pp. 2310–2321, Oct. 2007.

[22] H. Patel and V. Agarwal, "MPPT scheme for a PV-fed single-phase single-stage grid-connected inverter," IEEE Trans. Energy Convers., vol. 24, no. 1, pp. 256–262, Mar. 2009.

[23] J. Cao, N. Schofield, and A. Emadi, "Battery balancing methods: A comprehensive review," IEEE Veh. Power Propuls. Conf., pp. 1–6, 2008.

[24] S. Vijayakumar and N. Sudhakar, "Golden eagle optimized fractional-order PI controller for PFC SEPIC converter in EV charging," IEEE Access, vol. 12, pp. 102345–102356, 2024.

[25] R. Sharma, S. Chatterjee, and A. K. Rathore, "Coati optimized FOPID controller for non-isolated DC–DC converters in EV charging applications," IET Power Electron., vol. 17, no. 2, pp. 215–228, 2024.